EXTRACTION OF FLOOD-AFFECTED AGRICULTURAL LANDS IN THE GOOGLE EARTH ENGINE; CASE STUDY OF KHUZESTAN, IRAN

Parisa Dodangeh [1], Reza Shah-Hosseini [2] *

[1] PhD student, School of Surveying and Geospatial Engineering, College of Engineering, University of Tehran, Tehran.
[2] School of Surveying and Geospatial Engineering, College of Engineering, University of Tehran, Tehran.
(rshahosseini@ut.ac.ir)

Commission IV, WG IV/3

KEY WORDS: Google Earth Engine, Sentinel, Flood Mapping, Damage Assessment, Agriculture, Remote Sensing.

ABSTRACT:

Floods are one of the most dangerous crises that cause a lot of damage in various fields, including economic and human lives. Therefore, preparation for prevention and damage assessment in order to manage this crisis is essential. In the meantime, providing methods with high speed and accuracy together can be helpful. In this study, using the Google Earth engine system and various sources of remote sensing data, the flooded areas of 2019 in Khuzestan province of Iran were extracted and the area of damaged agricultural lands was estimated. The general method was to first use the Sentinel 1 images, which are independent of the cloud, and the JRC global surface water mapping data to obtain flooded areas. After that, with the help of Sentinel 2 images and extracting various features from its bands and implementing an automated method, a map of damaged agricultural lands was also prepared. In order to approximate the affected population, WorldPop Global Project Population data has been used to take advantage of the maximum capacity of various remote sensing sources. The resulting flood map was evaluated by a ground truth map to prove the efficiency of the method. The overall accuracy of the map was 96.30 and its kappa coefficient was 80.03, which is quantitatively appropriate. The proposed method and the system used, due to their simplicity, can be generalized at high speed to other areas.

1. INTRODUCTION

Flood is a sudden danger which causes great economic losses and victims all over the world. Therefore, accurate flood monitoring is essential for flood damage assessment and supportable planning to steer flood venture. In this area, satellite remote sensing is a low-cost tool that can be beneficially used for flood mapping (Notti et al., 2018). In the field of Earth Observations, late advances have dwindled the cost of flood mapping, which improves its accurate monitoring. Open accessing to different satellites such as Landsat and Sentinel is the first development. This has made it possible to map diverse natural phenomena with relatively high spatial and temporal resolution (Wulder et al., 2012). Second, it is possible to access and process large volumes of data along with the development of high-performance models using cloud computing platforms (Lewis et al., 2016). Google Earth Engine (GEE) is a platform developed by Google and has a wide range of capabilities in the field of earth data analysis on a global scale (Mehmood et al., 2021). GEE's free platform provides access to: (1) publicly availability of petabyte imageries and other products under the web application; (2) swift parallel processing and modern algorithms using Google's computational infrastructure; and (3) a library of Application Programming Interfaces (APIs) with environments that support popular coding languages. These important mentioned features provide users the possibility of remote sensing data analysis with powerful methods, while not requiring very strong hardware or professional programming knowledge (Tamiminia et al., 2020). Therefore, in conformity with the benefits of the Google Earth engine system and the demand for large-scale flood monitoring, in this research, GEE has been utilized to exert processes. The following is a summary of recent research on flood monitoring in the GEE to emphasize the notability of the issue. In 2020, Inman and Lyons provided an automatic procedure in GEE, including thresholding of the Landsat's SWIR band for classifying peak inundation in the Okavango Delta. Flood classification in the Okavango Delta was complicated by the spectral overlap between flooded areas covered by aquatic vegetation and dry vegetation classes in satellite images, and classifications have been mainly performed on wide spatial resolution images. They presented a long time series (1990–2019) of inundation maps for the peak flood season at 30-meter spatial resolution for the Delta. They also validated the maps using image-based and in situ data accuracy assessments, with overall accuracy ranging from 91.5% to 98.1% (Inman & Lyons, 2020). Singha et al. checked the spatiotemporal pattern of floods during 2014–2018, exploiting all the attainable Sentinel-1 images in GEE platform. They distinguished the flood-affected paddy rice fields by combining the flooding areas and remote sensing-based paddy rice planting areas. Between 2014 and 2018, the flood-affected paddy rice areas accounted for 1.61–18.17% of the total paddy rice area (Singha et al., 2020). In the following, Mehmood et al. utilized GEE and Landsat 5, 7, and 8 over a period of time for inundation identification. Their Flood Mapping Algorithm relied on expanding a "data cube", which is formed with the help of spatial overlapped Landsat images. This dataset was used to distinguish temporary and permanent water bodies using the Modified Normalized Difference Water Index (MNDWI), elevation and land use data. Their method had a high overall accuracy in the range of 74–89% (Mehmood et al., 2021). In order to flood intensity map preparation, Dodangeh et al. considered two time-series of radar and optic imageries

* Corresponding author

containing Sentinel-1 and Landsat-8 data in GEE and integrating statistical calculation and index extraction. In this study, first the permanent water surfaces automatically identified using optical imageries over a period of 5 years. Then, to determine the flood intensity in different regions, statistical calculations were used on the time series of radar images, and eventually, using the Normalized difference flood index (NDFI), which can quickly distinguish the flood, the final flood map was obtained. Assessments was done by ground truth maps in different sites, Golestan and Khuzestan province in Iran; The overall accuracy in a period of time in Golestan and Khuzestan was 91.84 and 97.36, which shows the method's good efficiency in distinct areas (Dodangeh et al., 2021). Pandey et al., in 2022, utilized Sentinel-1A data and GEE platform for flood extent estimation which for July–September was calculated to be 25,889.1 km^2 for Bangladesh. To extract the affected and damaged agricultural area and settlement, the Copernicus Global Land Cover dataset was used. The Gridded Population of the World (GPW) population density and Global Human Settlement Layer (GHSL) population dataset were also employed to evaluate flood impacts, which revealed that 23.29 million of the population was affected by floods in the Ganga-Brahmaputra basin (Pandey et al., 2022). Continuity and novelty of previous research indicate the importance of rapid and accurate flood monitoring.

In this study, the main purpose is to extract flooded areas and damage to agricultural areas along which the following sub-objectives are pursued: a) Use of GEE platform and satellite images with suitable spatial accuracy for rapid extraction of flooded areas and estimation of flooding area, b) Identify damaged agricultural areas, automatically, and c) An approximate estimate of the population affected by this disaster. The present paper includes sections as materials and methods, implementation and analysis of results and conclusion.

2. MATERIAL AND METHODS

2.1 STUDY AREA

The study area is parts of Khuzestan province in Iran, including the cities of Susangerd, Hamidiyeh, etc. which were flooded in April 2019 due to heavy rains. These areas were in the drainage basin of Karkheh and Dez rivers and are shown in Fig.1 with false bands composition including SWIR1, NIR, and red bands of Sentinel 2 plus Google earth image.

A

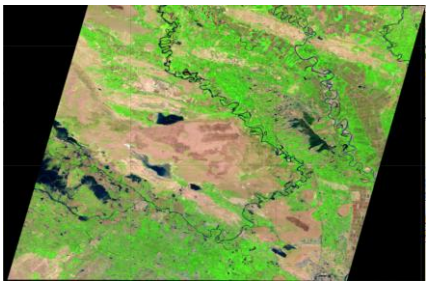

B

Figure 1. Study area; A) Google Earth image, B) Sentinel 2.

2.2 DATA

In this research, using different remote sensing images, an attempt has been made to produce a flood map with high accuracy and speed. Using the Google Earth Engine system allows a large volume of images to be processed in the shortest possible time. Here, a flood map was prepared using Sentinel-1 GRD images, and then the damage to the area was estimated with the help of Sentinel-2 images and WorldPop Global Project Population data. It should be noted that JRC global surface water mapping data has also been used to improve the flood map. To provide ground truth maps, Landsat 8 OLI image during flood period was used. Table 1 shows the information about the data used in this paper.

Satellite image	Date	Number
Sentinel 1 (before flood)	(2019-03-01) – (2019-03-15)	11
Sentinel 1 (after flood)	(2019-04-04) – (2019-04-10)	4
Sentinel 2	(2019-03-11) – (2019-03-20)	11
Landsat 8 OLI	2019-04-08	1
WorldPop Global Project Population	(2019-01-01) – (2020-01-01)	1

Table 1. Data used.

2.3 PROPOSED METHOD

The general process of conducting the research is presented in the Fig.2, which will be described in detail below. Initially, two collections of Sentinel 1 radar satellite imagery in two time periods before and after the flood were called in the Google Earth Engine environment. In particular, satellite-based synthetic aperture radar (SAR) systems have become a desirable tool for space-based flood mapping due to their 24-hour capabilities and acquisition in all weather conditions. (Dasgupta et al., 2018; Schumann & Moller, 2015). The initial flood map

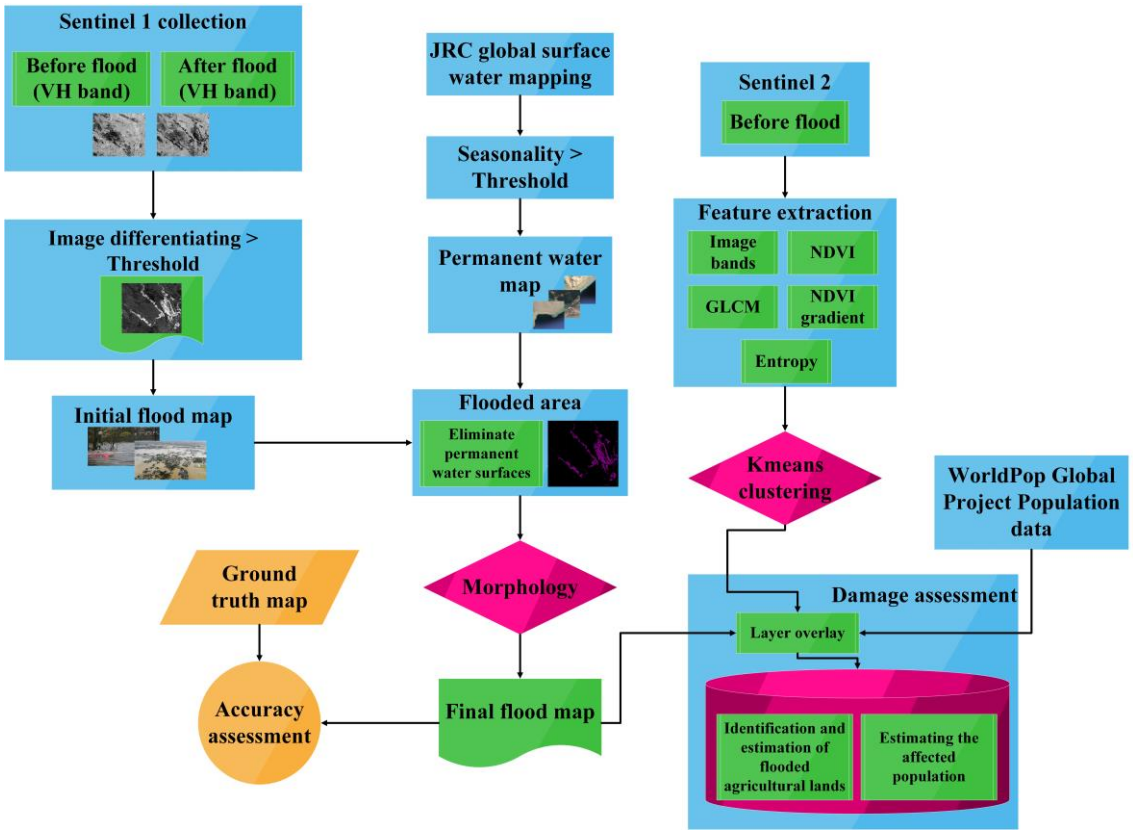

Figure 2. proposed method.

was obtained using the following equation, considering an experimental threshold.

$$Initialflood\_map = \frac{afterflood\_image}{beforeflood\_image} > Threshold \quad (1)$$

In the above equation, the VH bands of the images were selected due to their sensitivity to objects such as plants and water, and the speckle noise was removed. The threshold here was set at 1.2. This threshold can vary for different regions. Therefore, trial and error on its value by the researcher is necessary because the initial flood map will be the basis for further processing and its accuracy is very important. Although setting this threshold manually reduces the level of processing automation, but it was not time consuming.

The initial flood map includes all water areas, so with the help of JRC global surface water mapping data, which includes permanent water areas, these regions were removed from the map. Then, to further improve the flood map, morphological operations were used to eliminate some of the existing noise and misclassified areas. Thus, the flooded areas were extracted under the title of final flood map. Since the obtained map is the basis of further processing and achieving the research goal, it is therefore necessary to be evaluated by ground truth data. Ground truth map was visually prepared by the researcher from the Landsat 8 image.

Two other data sets including Sentinel 2 and WorldPop Global Project Population were used to assess the extent of damage in the region, especially in the agricultural and population sectors.

The flooded agricultural lands were estimated using pre-flood sentinel 2 images. On these optical images, a cloud filter of less than 5% was considered to prevent errors in the execution process. Feature selection is considered as an essential phase within a classification process because it meliorates the proficiency of the classifier and deduces the complexity of the computation by dispelling redundant information (Pedergnana et al., 2013). Feature selection has been greatly applied in remote sensing image classification (Ma et al., 2017). In this study, various features such as NDVI, NDVI Gradient, Entropy and GLCM were extracted from sentinel images. The NDVI is often used for change monitoring in land cover (Lunetta et al., 2006; Woodcock et al., 2002) and according to Singh et al. (Singh et al., 2016), this index produces a considerable betterment in accuracy (Tassi & Vizzari, 2020). In addition, Gray Level Co-Occurrence Matrix (GLCM) has proved to be a popular statistical method of extracting textural feature from images. According to co-occurrence matrix, Haralick (Haralick et al., 1973) defines fourteen textural features measured from the probability matrix to extract the characteristics of texture statistics of remote sensing images (Mohanaiah et al., 2013). From GLCM, four features as Angular Second Moment, Contrast, Correlation and Entropy were obtained from this matrix for use in research. A brief description of these 4 features is as follows:

- ASM: Measures the uniformity or energy of the gray level distribution of the image.
- Contrast: Measures the contrast based on the local gray level variation.
- Correlation: Measures the linear dependency of gray levels of neighbouring pixels.
- Entropy: Measures the degree of the disorder among pixels in the image (Tassi & Vizzari, 2020).

After extracting the mentioned features, these features form a stack with 14 bands with bands 2, 3, 4, 5, 6, 7, 8 and 11 of the Sentinel image. These bands are very effective in identifying areas with high greenery. Finally, a land use classification map was prepared using the Kmeans clustering algorithm with 5 classes. To calculate the damaged agricultural areas and the flood-affected population, a mask of the final flood map was prepared and applied to the Kmeans classification map and population data, thus performing the purpose of this study.
Although the proposed method is simple, it has a high computational speed, which proves its efficiency and positive performance in sensitive studies such as floods.

3. RESULTS

In this section, the items described in the previous section, their implementation and results are presented.

3.1 Flood maps generation

Here, we presented the images and results of flood monitoring. Fig.3 shows the before and after flood sentinel 1 images.

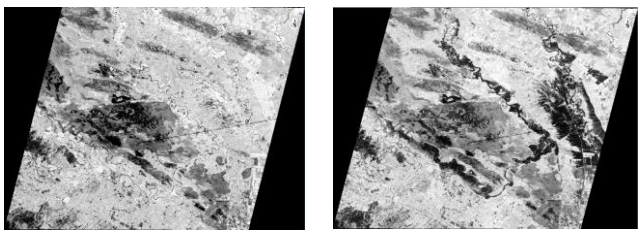

A B

Figure 3. Sentinel 1 images; A) before flood, B) after flood.

Flooded areas are well visible in Fig.3B in the dark. Fig.4 shows the difference image and the resulting initial flood map.

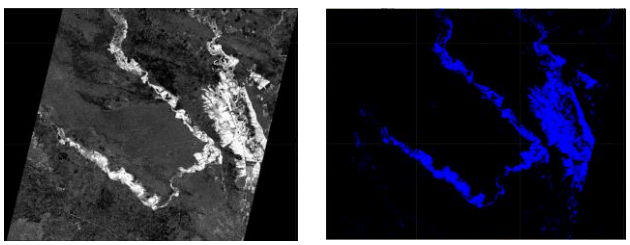

A B

Figure 4. Initial flood maps; A) difference image; B) difference image after thresholding (initial flood map).

In the pictures above, water surfaces such as permanent rivers can be seen. These regions should be removed to accurately estimate the amount of damage. Therefore, first, permanent water areas are eliminated by JRC data, and afterward morphological operations are performed on it for final flood map preparation. Fig.5 shows the results of this step.

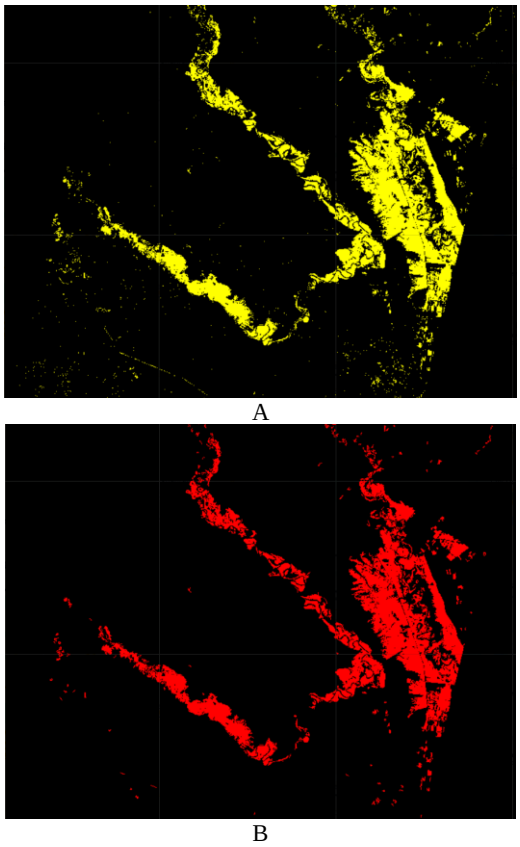

A B

Figure 5. Final flood maps; A) without morphology, B) with morphology.

As previously explained, the ground truth map of the flood was drawn with the knowledge of the researcher on the Landsat 8 false colour composite image. One of the reasons for using the Landsat image is the lack of a Sentinel 2 image during the flood period in the region. Also, because optical images are spectrally more suitable for visual recognition than radar data, optical imaging was used to provide this map. The ground truth map to assess accuracy is shown in Fig.6.

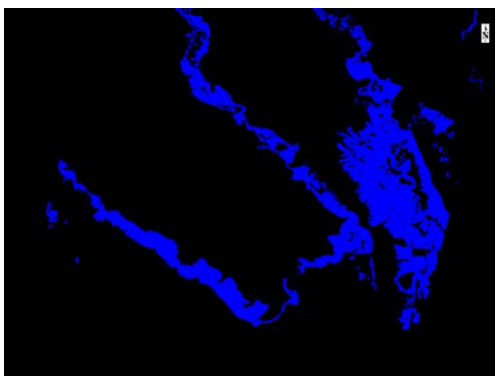

Figure 6. Ground truth map.

The studies performed by the accuracy assessment criteria are presented in Table 2.

Criterion \ Map	Without morphology	With morphology
Overall accuracy	96.26	96.30

This contribution has been peer-reviewed. The double-blind peer-review was conducted on the basis of the full paper.
https://doi.org/10.5194/isprs-annals-X-4-W1-2022-123-2023 | © Author(s) 2023. CC BY 4.0 License.

Kappa coefficient	79.94	80.03
F1_score	97.92	97.94
Commission error	3.85	3.82
Omission error	3.72	3.70

Table 2. Accuracy assessment.

The results of accuracy assessment indicate the appropriate quality of the proposed method. Also, according to the studied criteria, the impact of morphological operations can be helpful in eliminating noises although it didn't increase the accuracy perfectly. In addition, processing in the GEE system leads to a considerable increase in the speed of analysis and implementation.

3.2 Damage assessment

In this step, the flood map was first turned into a mask and then overlapped with the map obtained from Kmeans to identify damaged land uses. This map is presented in Fig.7.

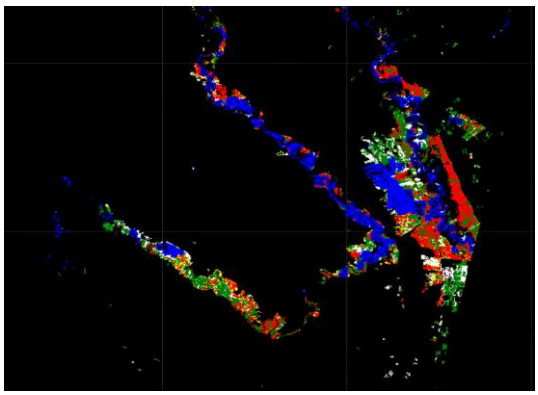

Figure 7. Flooded land uses.

From the above map, clusters related to agricultural areas are determined and separated from the rest, the result of which can be seen in Fig.8.

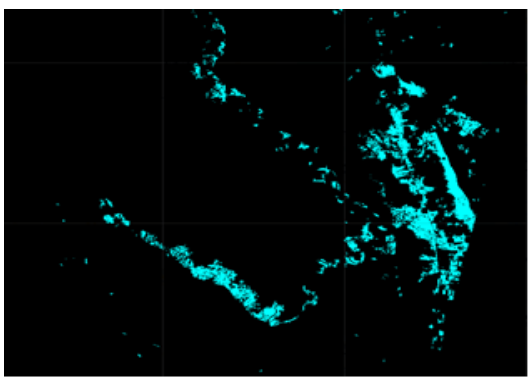

A

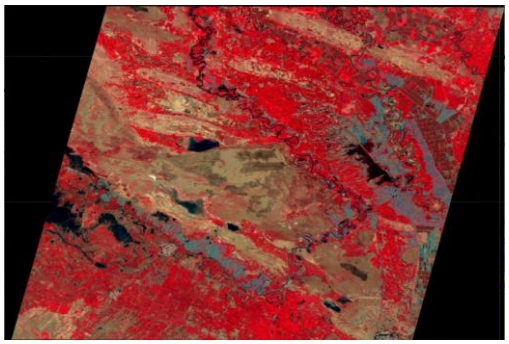

B

Figure 8. flood-affected agricultural lands.

Figure 8-A shows the binary map of the damaged agricultural areas and Figure 8-B shows the mask of these areas on the sentinel image before the flood. The goal is a better visualization. It should be noted that the false colour composite of the image includes Near-infrared, red and green bands.

The flooded regions area is estimated at 815 km^2 and the area of destroyed agricultural lands is estimated at 241 km^2. Also, the affected population estimated by WorldPop Global Project Population data was about 23,941 people. It should be noted that the data used to estimate the population has a spatial resolution of 92 meters, which is much less than the data used in previous sections. Therefore, the probability of error in this section is higher than others.

4. CONCLUSION

Floods are the uttermost repeated, fatal and incident natural perils of the world (Grimaldi et al., 2020). Earth observations can automatically support emergency management thanks to their synoptic view of the flooded area (Ajmar et al., 2017; Grimaldi et al., 2020). Therefore, in this research, using the Google Earth Engine system, which is able to process large volumes of satellite images, flood and damaged areas have been monitored. In this regard, various sources of satellite data including radar and optics have been used. This allows us to use these images without the need for heavy pre-processing. Then, a simple method based on radar satellite images was presented to prepare a flood map and the destroyed agricultural areas were examined by Sentinel 2 images. Population data in 2019 also provided an estimate of the flood-affected population. Assessing the accuracy of the map obtained with ground truth map indicates the performance efficiency of the proposed method. One of the challenges in this study is to identify areas that were not part of the flood but changed between the period before and after the flood. Therefore, this issue sensitizes the determination of flood detection threshold. One of the future goals is to improve this challenge by extracting interband features from Sentinel 1 images for better flooded area detection.

5. REFERENCES

Ajmar, A., Boccardo, P., Broglia, M., Kucera, J., Giulio-Tonolo, F., & Wania, A. (2017). Response to flood events: The role of satellite-based emergency mapping and the experience of the Copernicus emergency management service. *Flood Damage Surv. Assess. New Insights Res. Pract*, *228*, 213-228.

Dasgupta, A., Grimaldi, S., Ramsankaran, R., Pauwels, V. R., Walker, J. P., Chini, M., Hostache, R., & Matgen, P. (2018). Flood mapping using synthetic aperture radar sensors from local to global scales. *Global flood hazard: Applications in modeling, mapping, and forecasting*, 55-77.

Dodangeh, P., Ebadi, H., & Kiani, A. (2021). Identification of flooded areas using time series statistical calculations and based on integrating radar and optical data. *Iranian journal of Ecohydrology*, *8*(3), 623-639.

Grimaldi, S., Xu, J., Li, Y., Pauwels, V. R., & Walker, J. P. (2020). Flood mapping under vegetation using single SAR acquisitions. *Remote Sensing of Environment*, *237*, 111582.

Haralick, R. M., Shanmugam, K., & Dinstein, I. H. (1973). Textural features for image classification. *IEEE Transactions on systems, man, and cybernetics*(6), 610-621.

Inman, V. L., & Lyons, M. B. (2020). Automated inundation mapping over large areas using landsat data and google earth engine. *Remote Sensing*, *12*(8), 1348.

Lewis, A., Lymburner, L., Purss, M. B., Brooke, B., Evans, B., Ip, A., Dekker, A. G., Irons, J. R., Minchin, S., & Mueller, N. (2016). Rapid, high-resolution detection of environmental change over continental scales from satellite data–the Earth Observation Data Cube. *International Journal of Digital Earth*, *9*(1), 106-111.

Lunetta, R. S., Knight, J. F., Ediriwickrema, J., Lyon, J. G., & Worthy, L. D. (2006). Land-cover change detection using multi-temporal MODIS NDVI data. *Remote Sensing of Environment*, *105*(2), 142-154.

Ma, L., Fu, T., Blaschke, T., Li, M., Tiede, D., Zhou, Z., Ma, X., & Chen, D. (2017). Evaluation of feature selection methods for object-based land cover mapping of unmanned aerial vehicle imagery using random forest and support vector machine classifiers. *ISPRS International Journal of Geo-Information*, *6*(2), 51.

Mehmood, H., Conway, C., & Perera, D. (2021). Mapping of Flood Areas Using Landsat with Google Earth Engine Cloud Platform. *Atmosphere*, *12*(7), 866.

Mohanaiah, P., Sathyanarayana, P., & GuruKumar, L. (2013). Image texture feature extraction using GLCM approach. *International journal of scientific and research publications*, *3*(5), 1-5.

Notti, D., Giordan, D., Caló, F., Pepe, A., Zucca, F., & Galve, J. P. (2018). Potential and limitations of open satellite data for flood mapping. *Remote Sensing*, *10*(11), 1673.

Pandey, A. C., Kaushik, K., & Parida, B. R. (2022). Google Earth Engine for large-scale flood mapping using SAR data and impact assessment on agriculture and population of Ganga-Brahmaputra basin. *Sustainability*, *14*(7), 4210.

Pedergnana, M., Marpu, P. R., Dalla Mura, M., Benediktsson, J. A., & Bruzzone, L. (2013). A novel technique for optimal feature selection in attribute profiles based on genetic algorithms. *IEEE Transactions on Geoscience and Remote Sensing*, *51*(6), 3514-3528.

Schumann, G. J.-P., & Moller, D. K. (2015). Microwave remote sensing of flood inundation. *Physics and Chemistry of the Earth, Parts a/b/c*, *83*, 84-95.

Singh, R. P., Singh, N., Singh, S., & Mukherjee, S. (2016). Normalized difference vegetation index (NDVI) based classification to assess the change in land use/land cover (LULC) in Lower Assam, India. *International Journal of Advanced Remote Sensing and GIS*, *5*(10), 1963-1970.

Singha, M., Dong, J., Sarmah, S., You, N., Zhou, Y., Zhang, G., Doughty, R., & Xiao, X. (2020). Identifying floods and flood-affected paddy rice fields in Bangladesh based on Sentinel-1 imagery and Google Earth Engine. *ISPRS Journal of Photogrammetry and Remote Sensing*, *166*, 278-293.

Tamiminia, H., Salehi, B., Mahdianpari, M., Quackenbush, L., Adeli, S., & Brisco, B. (2020). Google Earth Engine for geo-big data applications: A meta-analysis and systematic review. *ISPRS Journal of Photogrammetry and Remote Sensing*, *164*, 152-170.

Tassi, A., & Vizzari, M. (2020). Object-oriented lulc classification in google earth engine combining snic, glcm, and machine learning algorithms. *Remote Sensing*, *12*(22), 3776.

Woodcock, C. E., Macomber, S. A., & Kumar, L. (2002). Vegetation mapping and monitoring. *Environmental modelling with GIS and remote sensing*, 97-120.

Wulder, M. A., Masek, J. G., Cohen, W. B., Loveland, T. R., & Woodcock, C. E. (2012). Opening the archive: How free data has enabled the science and monitoring promise of Landsat. *Remote Sensing of Environment*, *122*, 2-10.